Plasma Phys. Control. Fusion **50** (2008) 124002 (13pp) doi:10.1088/0741-3335/50/12/124002

High harmonics from solid surfaces as a source of ultra-bright XUV radiation for experiments

R Hörlein[1,2], Y Nomura[1], J Osterhoff[1], Zs Major[1,2], S Karsch[1], F Krausz[1,2] and G D Tsakiris[1]

[1] Max-Planck-Institut für Quantenoptik, Hans-Kopfermann-Strasse 1, D-85748 Garching, Germany
[2] Sektion Physik der Ludwig-Maximilians-Universität München, Am Coulombwall 1, D-85748 Garching, Germany

E-mail: george.tsakiris@mpq.mpg.de

Received 26 May 2008, in final form 23 June 2008
Published 3 November 2008
Online at stacks.iop.org/PPCF/50/124002

Abstract

The coherent high-order harmonic generation from the interaction of ultra-intense femtosecond laser pulses with solid density plasmas holds promise for tabletop sources of extreme ultraviolet (XUV) and soft x-ray radiation with attosecond duration and unprecedented intensities. Together with the generation of mono-energetic electron beams from gas jets and capillaries and the generation of mono-energetic ions from thin foils, this offers a unique tool box of tabletop-laser-generated radiation sources for a wide range of applications previously only accessible with large-scale accelerator and synchrotron-radiation facilities. Especially, the generation of high harmonics from laser plasmas has the potential of being applied to a wide range of experiments from plasma physics to molecular dynamics. So far the studies addressing the generation of high harmonics from laser-generated overcritical plasma surfaces have concentrated mainly on the characterization of the harmonic beams themselves not considering how, in a next step, these beams could be applied to experiments. In this paper we discuss the generation of surface harmonics with the ATLAS (800 mJ, 40 fs) laser system with the emphasis on the transport, spectral shaping refocusing of the harmonic beams, all of these being absolute prerequisites for multi-shot experiments. We also present considerations for future improvements and possible future experiments exploiting the full potential of high harmonic radiation from solid targets.

(Some figures in this article are in colour only in the electronic version)

1. Introduction

The generation of extreme ultraviolet (XUV) and soft x-ray (SXR) radiation both from large-scale synchrotron facilities and from the interaction of lasers with noble gases has

led to a wide range of new insights into the structure and dynamics of matter [1–3]. In particular, the generation of trains of [4] as well as of single [5] attosecond pulses from high harmonic generation in noble gases has opened an entirely new field in physics enabling measurements with unprecedented time resolution. The field of *attoscience* has allowed, for the first time, the direct observation of ultra-fast processes on the time scale of the electron motion in atoms [2, 3, 6]. While this technique is applied successfully in many laboratories its scope of applications is limited because the maximum achievable XUV energy is limited by the harmonic generation process itself [7]. Especially for the XUV-pump and XUV-probe type experiments and the imaging of single molecules [8] a higher photon flux is needed.

The generation of coherent high harmonics from the interaction of an ultra-intense laser pulse with a solid density plasma surface has the potential of overcoming this limitation and producing attosecond pulses of unprecedented intensities [9] that could be applied for a wide range of experiments. The unique combination of short wavelengths and very high time resolution should, for example, allow the probing of ultra-fast processes on the time scale of the plasma frequency in the evolution of high-density plasmas. For example, the current filamentation in solid density targets as well as its pre-plasma expansion could be visualized in real time [10, 11]. The second point could be especially of considerable interest for fast ignition inertial confinement fusion (ICF) studies [12].

Two distinct mechanisms for plasma surface high harmonic generation (SHHG) have been identified. For relativistic laser intensities, i.e. when $I\lambda^2 > 1.38 \times 10^{18}\,\mathrm{W\,cm^{-2}}\,\mu\mathrm{m}^2$, the dominant process is the frequency up-shifting of the incident laser light due to the reflection off the relativistically oscillating electron density surface, the relativistic oscillating mirror (ROM). This process is explained in detail by the theory of relativistic spikes of Baeva *et al* [13]. For sub- and moderately relativistic intensities the dominant mechanism is the coherent wake emission (CWE) described by Quéré *et al* [14]. Both these mechanisms are expected to generate coherent harmonics leading to temporal bunching and the generation of attosecond bursts of XUV radiation.

Many recent experiments have increased the insight into both SHHG mechanisms. In a series of measurements Dromey *et al* have shown harmonic spectra extending up to the keV photon energy range (approximately the 2800th order of the fundamental laser frequency) [15], the power-law roll-off of the harmonic spectrum in the relativistic regime [16] and the generation of diffraction limited harmonic beams at 40 nm wavelength [17]. Other experiments have led to new insights into the CWE mechanism, proving that the spectrum has a sharp cutoff related to the maximum density of the target and discussing the unequal temporal spacing of the individual emitted attosecond bursts [14, 18, 19].

Although all these experiments have led to a wealth of new insights into the generation mechanisms of high harmonics from plasma surfaces, they have all, up to now, focused on characterizing the generated harmonics. If one wants to take surface harmonics to the next level, i.e. to use the generated radiation in a variety of applications it becomes important to study issues such as transporting the beam, filtering the spectrum, suppressing the reflected infrared (IR) light from the target and accumulating many shots from a single target.

In this paper we address these issues in the discussion of an experimental setup recently installed in our laboratory designed for the study of non-linear processes in gases using high harmonics generated from solid targets.

2. Generation of harmonic XUV radiation from solid targets

High harmonics from various solid targets are routinely generated in our laboratory by focusing the 800 mJ, 40 fs pulses from the ATLAS Upgrade Titanium Sapphire laser system with a

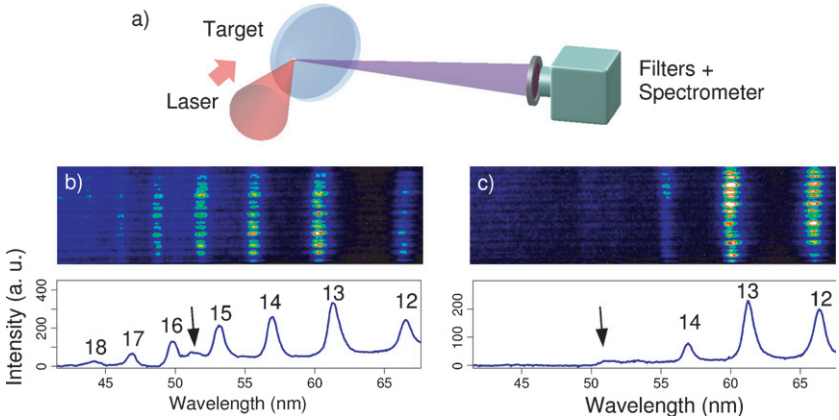

Figure 1. Sketch of the setup for surface harmonic generation and detection (*a*) and camera images and lineouts of measured harmonic spectra for two different target materials. The two spectra in this figure clearly show the difference in the emitted harmonic range for the two different target materials. While the spectrum in (*b*) for a BK7-glass target (density $\approx 2.7\,\mathrm{g\,cm^{-3}}$) extends up to the 18th harmonic, the PMMA target in (*c*) (density $\approx 1.2\,\mathrm{g\,cm^{-3}}$) shows a clear cutoff at the 14th. This corresponds nicely to the maximum plasma frequency in the ionized target. Both spectra are averages of 10 shots and were taken through an Al filter. The arrows mark the third order diffraction from an incoherent O_2 emission line at ≈18 nm. The horizontal lines in the spectra originate from the supporting mesh of the Al filter.

large-aperture $f/2.5$ off-axis parabola onto various solid targets. A sketch of this setup is shown in figure 1(*a*). The harmonic spectra are measured routinely using a 1 m focal length grazing incidence XUV spectrometer (McPherson Model 248/310) that can be equipped with a variety of thin metal filters. Two typical XUV spectra obtained from a high-density BK7 glass and a low-density polymethylmetacrylate (PMMA) target are shown in figures 1(*b*) and (*c*), respectively. Each spectrum is averaged over 10 shots and taken through a 150 nm thick aluminium filter.

The spectra obtained from the two different targets are qualitatively different. Both spectra extend to the respective cutoff harmonic order, q_{co}, expected from the CWE mechanism [14, 18]. While the PMMA spectrum extends to the 14th harmonic (H14) ($q_{\mathrm{co}}^{\mathrm{PMMA}} = \sqrt{n_{\mathrm{e,max}}^{\mathrm{PMMA}}/n_c} \approx \sqrt{200}$) the spectrum from the glass target extends up to H19 ($q_{\mathrm{co}}^{\mathrm{BK7}} = \sqrt{n_{\mathrm{e,max}}^{\mathrm{BK7}}/n_c} \approx \sqrt{400}$) (not on the record, see also figure 4(*a*)). The arrow between the H15 and H16 harmonic marks the third order diffraction of an incoherent emission line of oxygen.

Considering that the averaged focused intensity of our laser is $4 \times 10^{18}\,\mathrm{W\,cm^{-2}}$ in the $1/e^2$ radius and as high as $4 \times 10^{19}\,\mathrm{W\,cm^{-2}}$ in the peak, i.e. beyond the relativistic limit, it seems surprising at first glance that we observe this distinct CWE cutoff. In principle, our focused intensity is comparable to those achieved in other experiments [17, 18] where ROM harmonics were observed. The major difference between their experiments and ours is that we work at a peak-to-prepulse contrast of our laser that is roughly two orders of magnitude lower than in the other experiments owing to the fact that we do not use a plasma mirror (PM) [20] for contrast enhancement. Instead we rely on the relatively high inherent contrast of $10^{-8}:1$ at 4 ps before the main pulse of our ATLAS Upgrade laser system which is sufficient to generate harmonics reproducibly. This keeps the harmonic generation setup simple and robust, which is one of the most important features of a setup designed for pump–probe type experiments.

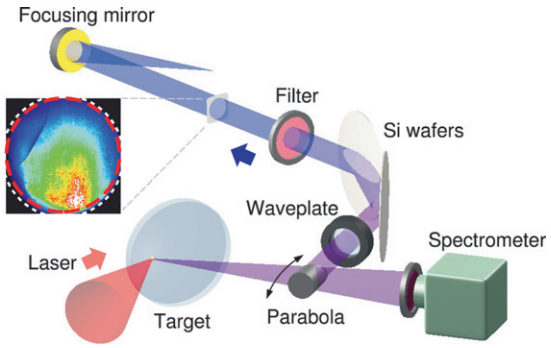

Figure 2. Schematic drawing of the setup used to transport and refocus the XUV beam for an application. The beam is recollimated using a gold-coated off-axis parabola, two silicon mirrors are used to efficiently suppress the residual IR and steer the beam that is subsequently filtered spectrally with a suitable metal filter and then refocused. The inlay shows a measured XUV beam profile (the dashed circle marks the size of the IR beam at the corresponding position of the setup).

Additionally the damage spots on the PM are much larger than those on the main target, which would again limit the number of shots that can be accumulated.

For many applications this limitation in the harmonic spectrum to photon energies up to the CWE cutoff does not pose a problem or may even be desirable when the XUV radiation is applied, for example, in two-photon ionization experiments such as in [21]. In such applications the cutoff can be utilized to suppress any radiation capable of ionizing the atoms to be studied with a single photon. This is of utmost importance since the cross section for single-photon ionization is orders of magnitude higher than that of the respective multi-photon process, which leads to the masking of the desired signal in the presence of photons with too high energies. In fact, in such experiments the CWE mechanism offers a convenient tool for tailoring the harmonic spectrum because cutoff orders between H12 for a low-density plastic target and H26, for example, from dense lead-glass can be selected and even higher cutoffs should be achievable with high-density metal targets.

To meet the demands of pump–probe type experiments regarding the accumulation of shots in one measurement we have constructed a special large-area target drive capable of holding 120 mm disc targets. This allows taking several thousands of shots before breaking the vacuum becomes necessary for target exchange, thereby ending the measurement. The exact number of shots depends strongly on the target material and the laser energy, both of which influence the size of the damage spot on the target. For a separation between shots of 1.5 mm, for example, 5000 shots can be taken.

3. Beam transport

The key to the successful application of the coherent XUV radiation routinely generated in our experiment is a robust and reliable beam transport system. The setup has to fulfil a series of requirements such as collimating the XUV beam, spectral filtering and especially suppressing the residual IR light. At the same time it is necessary to keep the number of reflections in the system as low as possible to minimize the losses during beam transport allowing for high XUV energies in the interaction region.

Figure 2 shows a schematic drawing of our current experimental setup. The harmonic beam generated from the target is recollimated using a 25 mm diameter 90° off-axis gold-coated parabola that can be removed from the beam to allow the measurement of the

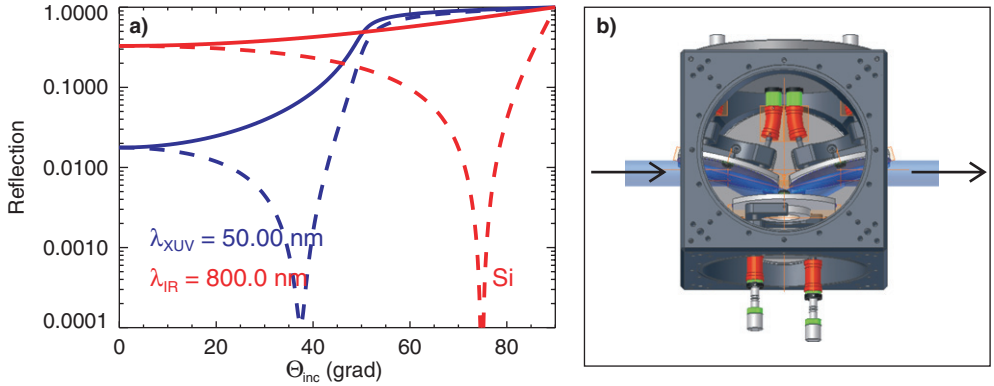

Figure 3. (*a*) Reflectivity of a silicon surface as a function of the incident angle in the IR (800 nm) and the XUV (50 nm). The dashed curve is for p while the solid curve is for s polarization. The strong suppression of the 800 nm radiation at the Brewster angle of 75° is clearly visible for p-polarized light. In (*b*) we show a technical drawing of our mobile IR suppression unit. It is fitted into a $20 \times 20 \times 20\,\mathrm{cm}^3$ vacuum cube that can be installed at various positions in the experimental setup.

XUV spectrum. The IR fundamental laser radiation is strongly suppressed using two Brewster angle reflections on large-aperture silicon mirrors before the beam is spectrally filtered using thin metal foils. A half-wave plate can be inserted into the beam to rotate the polarization of the IR beam, thus increasing the reflectivity of the Si wafers to make the alignment with a low-energy beam possible. Finally the beam is focused for application. If the pump–probe capability of the setup is desired, the focusing mirror can be replaced, for example, by a split-mirror setup such as the one used in [21] acting as an XUV beam splitter. The inset in figure 2 shows an XUV beam profile measured at the position depicted in the figure. The dashed circle indicates the size of the IR beam measured with a caesium–iodine multi-channel plate at the same position.

3.1. IR suppression

Owing to the high laser energies used in the generation of the harmonics it is very important to suppress the IR radiation efficiently before sending the beam through a metal filter to prevent damaging it. It is also important to note that the method often employed in gas harmonic experiments of placing a beam block in the central part of the focusing laser and thus generating an annular IR beam after the target [22] that can in turn be blocked with a complementary mask does not work for surface harmonics because the generation mechanism itself behaves like an efficient spatial filter [23, 24].

A convenient solution to this problem is the reflection of the beam from a Si surface under the Brewster angle for IR radiation [25]. Especially for Si the ratio between the XUV and IR reflectivity is very advantageous. At the same time large-aperture Si wafers are readily available because of their importance in chip production. Figure 3(*a*) shows the reflectivity of Si for IR and XUV radiation as a function of the incidence angle and the polarization. Note the suppression of the fundamental for the 75° angle of incidence. While the calculation shown in figure 3 was done for a single wavelength it is important to point out that for a pulse of 30 nm spectral bandwidth the theoretically achievable suppression is still better than $10^4 : 1$ for a single reflection. In our experiment we implement the Si mirrors either in the configuration

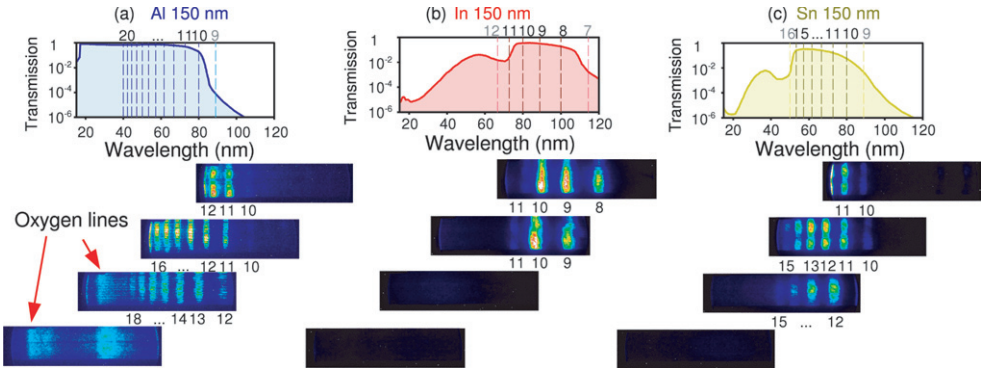

Figure 4. Reference transmission curves (from [26, 27]) and the XUV spectra measured through 150 nm thick filters of (*a*) aluminium, (*b*) indium and (*c*) tin. The spectra were taken at four different wavelength settings of the XUV spectrometer and can be directly compared for the various materials.

shown in figure 2 or in a separate IR suppression unit (right image in figure 3) that can be modularly inserted into any setup without altering the beam path.

Also one is not restricted to silicon for IR suppression. As shown later, we have also implemented a fused silica wedge for IR suppression. While the reflectivity for XUV is slightly lower in that case the main advantage lies in the fact that very high quality quartz surfaces are readily available due to their importance as mirror substrates.

3.2. Spectral filtering

After the suppression of large parts of the IR radiation a thin metal filter can safely be placed in the beam to select the desired spectral region from the XUV beam. Depending on the exact application and the generated harmonic spectrum a wide range of materials can be applied. In figure 4 we illustrate the influence of different filter materials on the harmonic spectrum by comparing the measured XUV spectra with the reference transmission curves taken from [26, 27] for different thin metal filters. Good agreement between the reference and our spectra is found in the measurement. For an overview of the expected attosecond pulse duration achievable for beams filtered with various materials see [9].

In addition, and especially in those wavelength ranges for which no appropriate filter material is available, XUV and SXR multi-layer mirrors [28] can help to confine the spectrum to the desired wavelength range.

4. Characterization of the beam transport system

To further characterize our setup we have conducted a series of measurements to study some of the key issues that need to be addressed when planning an experiment with the generated XUV radiation. In the following subsections we discuss two especially important points: the absolute XUV pulse energy available after IR suppression and spectral selection and the stability of the XUV signal.

4.1. Conversion efficiency

While spectral filtering and IR suppression can be achieved with the methods discussed in the previous section one very important point has not been discussed so far: how much XUV energy is transmitted through the setup and is thus available for an application after the beam

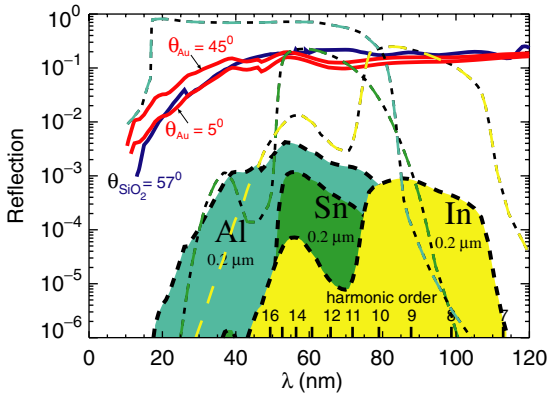

Figure 5. Transmission curves of the whole setup assuming ideal reflectivities of the mirrors (the reference values for the complex index of refraction were taken from [29]) and the filter transmission values [26, 27]. The solid lines show the reflectivity of the recollimating parabola (AOI 45°), the split mirror (AOI 5°) and the reflectivity of the quartz wedge used for IR suppression as a function of the XUV wavelength. Transmission curves of the individual filters are shown using dashed lines. The overall transmission of the whole system is indicated by the filled areas.

has passed the optical components for spectral shaping? Therefore, the absolute XUV energy and subsequent focused intensity in the interaction region need to be investigated. In particular, if the harmonic beam is to be applied for triggering a non-linear process a minimum XUV intensity and signal stability is an essential prerequisite.

To study this we have conducted measurements of the XUV pulse energy using an absolutely calibrated large area XUV diode placed behind the thin metal filter (see figure 2). In our measurements we obtain an XUV pulse energy of 13.5 nJ after the reflection of the harmonics generated from PMMA off the 90° gold-coated off-axis parabola with a protective coating, a quartz substrate under 57° angle of incidence (AOI) (this replaced the two silicon wafers for IR suppression in this experiment) and the transmission through 150 nm of indium foil. Figure 5 shows the calculated reflectivities and transmissions for the quartz plate, the gold mirrors and three different filter materials. The expected throughput from the source to the focus for the various filters is shown in the filled graphs.

Assuming theoretical values for the reflectivities of gold and quartz under the respective angles of incidence and the transmission of the filter it is possible to estimate the conversion efficiency into H8 to H14. This estimate, using the values depicted in figure 5, yields a lower limit of 6×10^{-5} corresponding to 40 μJ of pulse energy at the target. It is important to emphasize, however, that this is the absolute lower limit and the real value could easily be as high as 1×10^{-3} because neither the protective coating on the gold parabola nor possible contaminations on the surfaces of the optics were taken into account.

From the measured XUV energy we can also estimate the focused intensity of the harmonic beam. Up to now we have used a near normal incidence reflection off a spherical gold mirror to accomplish this. While this is the simplest approach it is also the least efficient. The reflectivity is rather low under normal incidence and the focal spot quality is degraded due to spherical aberrations in the focus. Even though there is still a lot of room for improvement, simulations of the focal spot have shown that we can achieve focused XUV intensities of $(0.5–1) \times 10^{11}$ W cm^{-2} in our setup.

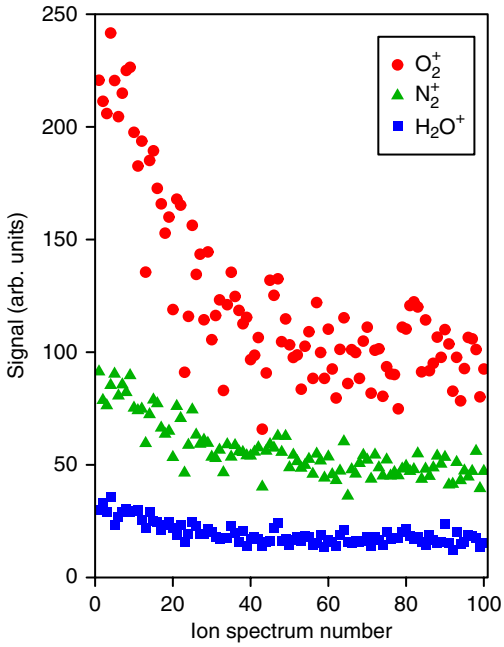

Figure 6. The ion yield of various molecules measured with a TOF spectrometer as a function of ion spectrum number on the target. Each ion spectrum in turn consists of 20 individual shots. For these measurements the XUV radiation from the target was spectrally filtered with an In filter and then focused in vacuum in our ion TOF spectrometer. All ions originate from single photon ionization of the residual background gas. The decay in the ion signal is thus directly related to the XUV yield from the target and shows obvious degradation of the emission with shot number due to debris deposition on the target.

4.2. Stability of the XUV signal

The second important aspect when applying the generated harmonics to any kind of experiments is the stability and reproducibility of the harmonic spectrum. While the range of generated harmonics is very stable under our experimental conditions the shot-to-shot fluctuation of the XUV pulse energy remains to be investigated. To study this in detail we have conducted an experiment in which we focused our harmonic beam after spectral selection with a PMMA target and a 150 nm indium filter thus selecting H8–H10 with some additional contribution of H11–H14 into a He gas jet, which was originally set up for two-photon ionization measurements, and measured the yield of contamination ions using a time-of-flight (TOF) spectrometer. The ion yield for various contamination ions as a function of the ion spectrum number for the first 100 spectra (where each spectrum is the accumulation of 20 individual shots) on a fresh PMMA target is shown in figure 6. It is important to note that the photon energies of H8–H14 are all energetic enough to ionize H_2O and O_2 with a single photon (ionization potentials are 12.6 eV and 12.1 eV, respectively [30]) so that the measured ion yield is directly proportional to the XUV energy. For N_2 only harmonics 11 and up (ionization potential is 15.6 eV [30]) contribute to the signal explaining why the signal is lower even though nitrogen is expected to be the main component of the background gas.

Two different types of energy fluctuations can be observed in the measurement: fluctuations between neighbouring data points and a longer-term degradation with subsequent leveling off of

the signal. On the one hand, the short-term fluctuations most likely originate from shot-to-shot energy fluctuations of our laser and varying pre-pulse levels and cannot be avoided easily. However, they can be dealt with by averaging the measured signal in an application over more shots if necessary. The long term degradation on the other hand most probably originates from the degradation of the target surface due to deposition of debris from previous shots on the clean surface. This would lead to an increasing surface roughness of the target over time and subsequent signal degradation. Detailed studies of the influence of surface roughness on harmonic generation have been conducted previously [17]. To some extent this degradation can be influenced by the choice of the target material, e.g. we found that a PMMA target degrades faster than a BK7 target, but a complete suppression of the degradation is not possible with large-area disc targets.

Ultimately this problem can only be solved by designing special target mechanisms that efficiently protect the fresh target from debris. In this context, tape targets could be applied for certain target materials, e.g. plastic or metals. The best solution could be the replacement of the solid target with a liquid jet, where a fresh target could be supplied for as many shots as necessary.

5. Optimized setup

The two aforementioned factors, the XUV focal spot quality and the throughput of the beamline, are the two things that need to be improved for an optimized experimental setup that makes the best possible use of the generated XUV radiation. To improve the XUV focusing the only solution is to go from a spherical focusing optic to either a parabolic or an elliptical one. This not only improves the quality of the focus but is also absolutely necessary for optimizing the throughput. In order to increase the reflectivities the most important step is to make the angles of incidence as large as possible to take advantage of the inherently higher reflectivities for grazing-incidence reflections. At the same time this requires non-spherical surfaces to minimize aberrations and keep the resulting focal spot small. This in conjunction with the use of optimized coatings (for example, XUV multi-layers or certain metals such as tungsten or osmium) for the desired wavelength range will allow one to explore the full potential of the surface harmonics by minimizing the losses during beam transport.

In figure 7 we propose possible optimized setups for two experimental scenarios. While the proposed configuration in figure 7(*a*) with two large AOI off-axis parabolas for recollimation and subsequent aberration-free focusing is optimized for XUV-pump–XUV-probe type experiments using a split mirror, the second setup (figure 7(*b*)) using an elliptical mirror for point-to-point imaging is ideal if a single XUV beam of maximum intensity is desired because the number of reflections is minimized in this scheme. Note that both setups are in one plane and subsequently both the IR and the XUV beam are p polarized on all optics.

In order to decide what kind of angles of incidence to use several factors have to be taken into account. On the one hand, it is desirable to make the angle as large as possible but, on the other hand, the feasible mirror sizes and beam diameters after collimation in scheme (*a*) are limited. Moreover the distance between the target and the mirror has to be sufficiently large so that the residual IR beam has expanded far enough to not damage the mirror coating. The decision also depends on the harmonics used since the divergence depends strongly on harmonic order and the generation mechanism. In the end the decision has to be taken for every harmonic range separately since it is based on many parameters of the specific experiment.

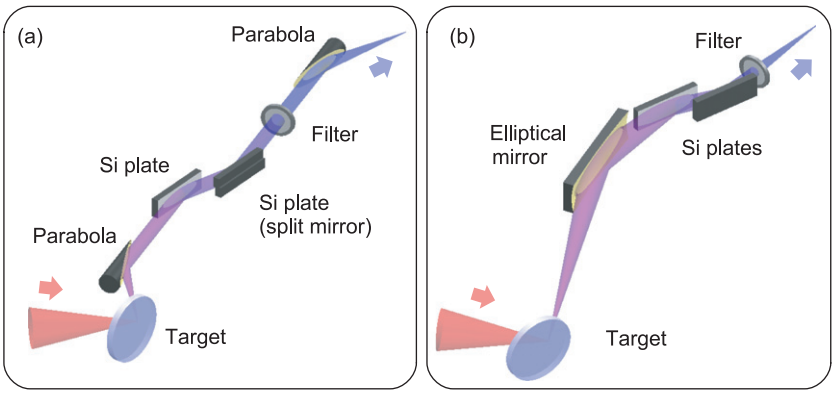

Figure 7. Two possible improved experimental setups for XUV beam delivery to an experiment. Setup (*a*) shows an optimized XUV-pump–XUV-probe experiment where a split mirror is needed to introduce a delay between two parts of the pulse. Setup (*b*) is designed for maximum XUV throughput by using an elliptical mirror for point-to-point imaging and minimizing the number of reflections in the beam path.

Taking all the considerations for the optimized setup into account the throughput of the system for the H-8–H-14 investigated in section 4 could be increased by a factor of 5 for scheme (*a*) and by roughly 25 for scheme (*b*). Together with the optimized focusing properties of the setups this makes increases in focused XUV intensities by up to 3 orders of magnitude for the same source seem feasible. Even higher values should be achievable when the focusing optics are placed such that the XUV beam on them is s polarized. The obvious disadvantage of this is that the beam path is not in one plane anymore making the setup and alignment even more difficult.

It is important that this scheme is obviously not limited to the rather low photon energies currently accessible in our experiment. When using optimized multi-layer coatings an even higher throughput seems feasible in the 100 eV photon energy range due to the optimized reflectivities of the coatings albeit limiting the spectral range.

6. Conclusions and outlook

In conclusion we have successfully demonstrated an experimental setup that is capable of delivering up to 5000 bursts of coherent XUV radiation and pulse energies in excess of 10 nJ to the focusing optic of an experiment at a 10 Hz repetition rate. We have characterized the beam spectrally, spatially as well as with respect to the shot-to-shot and long-term signal stability. Furthermore we have discussed spectral filtering and the suppression of residual IR radiation using metal filters and Brewster angle reflections.

Optimization of the beam transport setup will allow one to increase the XUV pulse energy available for application towards the microjoule range and allow for focused intensities as high as $10^{14}\,\mathrm{W\,cm^{-2}}$ with driving lasers such as the one used in these experiments. Our experiments show that it is feasible to not only generate harmonic spectra from solid targets with unprecedented intensities much higher than those achievable from gaseous media but also deliver these to an experimental setup. Furthermore, they define the prerequisites and the technical background for taking advantage of the fast advancing high-power tabletop laser system development to generate intense attosecond pulses that have been predicted by PIC simulations [9] using these laser systems. This will open the path to a host of femtosecond

and possibly attosecond time resolution experiments not accessible with low intensity gas-harmonic sources.

To date, attosecond pulses are generated in atomic media, but the low number of photons has limited their use to triggering or to probing fast evolving dynamical processes. Making the most of the full potential of attosecond technology calls for attosecond pulses being intense enough to be simultaneously used as a pump for triggering a fast dynamic process and as a probe for following its unfolding. Scaling waveform controlled few-cycle laser pulses to relativistic intensities and the use of the plasma medium appear to be the only viable ways for producing high-intensity attosecond photon pulses in the XUV and SXR regimes that can be simultaneously applied for both purposes [31]. The unique combination of a high photon flux, wide tunability of the available fs-duration XUV pulses, the capability of generating broad-band attosecond pulses and the inherent optical synchronization between the XUV bursts and a high-intensity IR-pulse makes such a setup a unique tool combining the time resolution and tunability of gas-harmonic sources with the high photon flux only achievable so far at large-scale facilities.

The impact that the availability of an intense light pulse with duration approaching the atomic time scale would have is manifested in the number of reports that have recently appeared. They describe possible applications of this extraordinary light flash to investigations of processes from various fields of physics unfolding on the femto- or attosecond time scale. In plasma physics, they would enable real-time probing of dynamical processes on the time scale of the local plasma frequency in high-density plasmas. For example, it is envisioned to follow the development of the filamentation instability arising in the propagation of mega-ampere current in dense plasmas as those encountered in the fast ignition concept using synchronized attosecond x-ray pulses [32]. Details of the temporal evolution of the wake field used for tabletop plasma accelerators are essential for the optimum control and optimization of the process [33]. The high time resolution afforded by XUV attosecond pulses holds the promise of a direct observation of the accelerated electrons as they fill the potential bucket and of the resulting wave-breaking.

In atomic physics, intense attosecond pulses are in demand to shed light onto one of the most fundamental processes: the non-sequential two-photon double ionization of helium. The XUV-pump–XUV-probe experiment is expected to provide an important insight into the role of electron–electron correlation in the full three-body nature of the breakup process [34–37]. The real-time observation of the ultra-fast changes occurring at surfaces is another field that would considerably benefit from the availability of intense XUV attosecond pulses. Ultraviolet photoelectron spectroscopy would enable a direct access to much deeper electron levels while providing unprecedented temporal resolution [38, 39].

The most promising route to all these goals is to expose a solid surface to relativistic-intensity light thus generating attosecond pulses with a sufficient number of photons to trigger a reaction and follow up its evolution. In this respect, the efficient transport, spectral selection and purification of these number of photons from the source to the application are of paramount importance.

Acknowledgments

The authors gratefully acknowledge the help of P Tzallas and B Dromey and would like to thank D Charalambidis for helpful discussions. This work was supported in part by the DFG-Projects Transregio 18 and MAP, by the European Community's Human Potential Programme under Contract MRTN-CT-2003-505138 (XTRA) and by the association EURATOM-Max-Planck-Institut für Plasmaphysik.

References

[1] Zou P, Pinotsis N, Lange S, Song Y-H, Popov A, Mavridis I, Mayans O M, Gautel M and Wilmanns M 2006 Palindromic assembly of the giant muscle protein titin in the sarcomeric z-disk *Nature* **439** 229–33

[2] Cavalieri A L *et al* 2007 Attosecond spectroscopy in condensed matter *Nature* **449** 1029–32

[3] Uiberacker M *et al* 2007 Attosecond real-time observation of electron tunnelling in atoms *Nature* **446** 627–32

[4] Agostini P and DiMauro L F 2004 The physics of attosecond light pulses *Rep. Prog. Phys.* **67** 813–55

[5] Sansone G *et al* 2006 Isolated single-cycle attosecond pulses *Science* **314** 443–6

[6] Drescher M, Hentschel M, Kienberger R, Uiberacker M, Yakovlev V, Scrinzi A, Westerwalbesloh Th, Kleineberg U, Heinzmann U and Krausz F 2002 Time-resolved atomic inner-shell spectroscopy *Nature* **419** 803–6

[7] Brabec T and Krausz F 2000 Intense few-cycle laser fields: frontiers of nonlinear optics *Rev. Mod. Phys.* **72** 545–91

[8] Chapman H N *et al* 2007 Femtosecond time-delay x-ray holography *Nature* **448** 676–9

[9] Tsakiris G D, Eidmann K, Meyer-ter-Vehn J and Krausz F 2006 Route to intense single attosecond pulses *New J. Phys.* **8** 19

[10] Theobald W, Häßner R, Wülker C and Sauerbrey R 1996 Temporally resolved measurement of electron densities ($>10^{23}$ cm^{-3}) with high harmonics *Phys. Rev. Lett.* **77** 298–301

[11] Honrubia J J and Meyer-ter-Vehn J 2006 Three-dimensional fast electron transport for ignition-scale inertial fusion capsules *Nucl. Fusion* **46** L25–8

[12] Tabak M, Hammer J, Glinsky M E, Kruer W L, Wilks S C, Woodworth J, Campbell E M, Perry M D and Mason R J 1994 Ignition and high gain with ultra-powerful lasers *Phys. Plasmas* **1** 1626

[13] Baeva T, Gordienko S and Pukhov A 2006 Theory of high-order harmonic generation in relativistic laser interaction with overdense plasma *Phys. Rev.* E **74** 046404

[14] Quéré F, Thaury C, Monot P, Dobosz S, Martin P, Geindre J-P and Audebert P 2005 Coherent wake emission of high-order harmonics from overdense plasmas *Phys. Rev. Lett.* **96** 125004

[15] Dromey B *et al* 2007 Bright multi-kev harmonic generation from relativistically oscillating plasma surfaces *Phys. Rev. Lett.* **99** 085001

[16] Dromey B *et al* 2006 High harmonic generation in the relativistic limit *Nature Phys.* **2** 456–9

[17] Dromey B *et al* 2008 Diffraction limited performance and focusing of high harmonics from relativistic plasmas submitted

[18] Thaury C *et al* 2007 Plasma mirrors for ultrahigh-intensity optics *Nature Phys.* **3** 424–9

[19] Quéré F, Thaury C, Geindre J-P, Bonnaud G, Monot P and Martin Ph 2008 Phase properties of laser high-order harmonics generated on plasma mirrors *Phys. Rev. Lett.* **100** 095004

[20] Kapteyn H, Murnane M, Szoke A and Falcone R 1991 Prepulse energy suppression for high-energy ultrashort pulses using self-induced plasma shuttering *Opt. Lett.* **16** 490

[21] Tzallas P, Charalambidis D, Papadogiannis N A, Witte K and Tsakiris G D 2003 Direct observation of attosecond light bunching *Nature* **426** 267–70

[22] Peatross J, Chaloupka J L and Meyerhofer D D 1994 High-order harmonic generation with an annular laser beam *Opt. Lett.* **19** 942–4

[23] Moncur K 1977 Plasma spatial filter *Appl. Opt.* **16** 1449

[24] Hörlein R, Dromey B, Adams D, Nomura Y, Kar S, Markey K, Foster P S, Neely D, Krausz F, Tsakiris G D and Zepf M 2008 High contrast plasma mirror: spatial filtering and second harmonic generation at 10^{19} W cm^{-2} *New J. Phys.* at press

[25] Takahashi E J, Hasegawa H, Nabekawa Y and Midorikawa K 2004 High-throughput, high-damage-threshold broadband beam splitter for high-order harmonics in the extreme-ultraviolet region *Opt. Lett.* **29** 507–9

[26] Gullikson E M X-ray interaction with matter http://www-cxro.lbl.gov/optical_constants

[27] Henke B L, Gullikson E M and Davis J C 1993 X-ray interactions: photoabsorption, scattering, transmission, and reflection at $e = 50$–$30\,000$ eV, $z = 1$–92 *At. Data Nucl. Data Tables* **54** 181–342

[28] Spiller E 1994 *X-Ray Optics* (Bellingham, WA: SPIE Optical Engineering Press)

[29] Palik E D (ed) 1985 *Handbook of Optical Constants of Solids I and II* (New York: Academic)

[30] Lidle D R (ed) 2004 *CRC Handbook of Chemistry and Physics* 85th edn (Boca Raton, FL: CRC Press)

[31] Corkum P B and Krausz F 2007 Attosecond science *Nature Phys.* **3** 381–7

[32] Meyer-ter Vehn J, Honrubia J, Geissler M, Karsch S, Krausz F, Tsakiris G and Witte K 2005 On electron transport in fast ignition research and the use of few-cycle pw-range laser pulses *Plasma Phys. Control. Fusion* **47** B807–13

[33] Matlis N M *et al* 2006 Snapshots of laser wakefields *Nature Phys.* **2** 749–53

[34] Hu S X and Collins L A 2006 Attosecond pump probe: exploring ultrafast electron motion inside an atom *Phys. Rev. Lett.* **96** 073 004
[35] Morishita T, Watanabe S and Lin C D 2007 Attosecond light pulses for probing two-electron dynamics of helium in the time domain *Phys. Rev. Lett.* **98** 083003
[36] Foumouo E, Antoine P, Bachau H and Piraux B 2008 Attosecond timescale analysis of the dynamics of two-photon double ionization of helium *New J. Phys.* **10** 025017
[37] Feist J, Nagele S, Pazourek R, Persson E, Schneider B I, Collins L A and Burgdörfer J 2008 Nonsequential two-photon double ionization of helium *Phys. Rev.* A **77** 043420
[38] Bauer M 2005 Femtosecond ultraviolet photoelectron spectroscopy of ultra-fast surface processes *J. Phys.D: Appl. Phys.* **38** R253–67
[39] Bovensiepen U 2007 Coherent and incoherent excitations of the Gd(0 0 0 1) surface on ultrafast timescales *J. Phys.: Condens. Matter* **19** 1–55